CRYSTAL GROWTH & DESIGN
2009
VOL. 9, NO. 1
210–217

Shape Control of Cobalt Carbonate Particles by a Hydrothermal Process in a Mixed Solvent: An Efficient Precursor to Nanoporous Cobalt Oxide Architectures and Their Sensing Property

Huai-Ping Cong and Shu-Hong Yu*

Division of Nanomaterials and Chemistry, Hefei National Laboratory for Physical Sciences at Microscale, Structural Research Laboratory of CAS, Department of Materials Science and Engineering, University of Science and Technology of China, Hefei 230026, P.R. China

Received March 22, 2008; Revised Manuscript Received September 26, 2008

ABSTRACT: Shape-controlled synthesis of $CoCO_3$ crystals has been achieved by a hydrothermal process in a mixed solvent of water and ethanol (or glycerol). Uniform $CoCO_3$ crystals with novel structures can be fabricated by tuning the volume ratio of water and ethanol (or glycerol). The results demonstrated that the as-prepared $CoCO_3$ crystal can act as an efficient precursor for production of nanoporous Co_3O_4 particles with pore sizes of 2.5 and 60 nm by calcination at 500 °C. The nanoporous Co_3O_4 particles show sensitive response and reversibility in sensing performance.

1. Introduction

Research on nanomaterials has been persistent due to their unique optical, electrical, magnetic, and catalytic properties compared with those of the bulk materials. Recently, more and more attention has been paid to the control of the morphologies and the microstructures of materials, because the materials with novel functionalities depend not only on the compositions but also on the shapes and sizes. Compounds with the same compositions but different morphologies and microstructures exhibit substantial differences in properties.[1−5] Up to now, various methods have been used to synthesize different kinds of nanomaterials with unique morphologies and special structures, including nanowires,[6] nanorods,[7] naotubes,[8] nanobelts,[9] nanoplates,[10] nanorings,[11] nanoparticles,[12] and other nanostructures.[13]

Metal carbonate is an important class of the inorganic materials and is used as the standard model system due to its abundance in nature and the wide applications in industry, such as paints, plastics, rubbers, and papers.[14] Crystallization of the biomineral $CaCO_3$ has been intensively studied in recent years as reviewed.[15] Also, other metal carbonates such as $BaCO_3$,[16] $CdCO_3$,[17] $MnCO_3$,[17a,18] and $PdCO_3$[17a] have also been synthesized by mineralization approaches. It has been pointed out that mineralization of inorganic minerals usually has been carried out in aqueous solution. A few reports demonstrated that mineralization reactions in nonaqueous solution such as in alcohol, ethanol, 2-propanol, and diethylene glycol can vary the shape of $CaCO_3$ crystals and phases.[19] Polymer-controlled crystallization in a mixed solvent[20] or in nonaqueous solution[21] can result in entirely distinct results due to the changes in precursor solubility, precipitation kinetics, solution property, and aggregation forms of the polymer in a mixed solution. However, to the best of our knowledge, controlled synthesis of cobalt carbonate with novel structures and uniform shapes has been rarely studied.[22]

Spinel Co_3O_4 is an important p-type semiconductor due to its potential applications as a solid-state sensor,[23] a heterogeneous catalyst,[24] an electrochemical device,[25] energy storage,[26] and a rotatable magnet.[27] Recently, more effort has been focused on the fabrication of cobalt oxide with novel nanostructures, such as nanocubes,[28] nanofibers,[29] nanotubes,[30] nanorods,[31] nanowalls,[32] nanoboxes,[33] hollow spheres,[34] and porous nanostructures.[35] Among the synthesis methods of this material is a two-step route to fabricate Co_3O_4 crystals with different shapes and novel structures; that is, the precursor compounds are synthesized in the first step, and then the precursor is calcinated to produce Co_3O_4. Cobalt hydroxide as the precursor has been used to prepare uniform Co_3O_4 nanoplates and flowers.[36] A so-called polyol process has been developed for synthesizing Co_3O_4 with hierarchical structures by Cao et al.[37] Co_3O_4 nanorod bundles have been synthesized from a single precursor $[Co(CO_3)_{0.35}Cl_{0.20}(OH)_{1.10}]$.[38] Recently, Han et al. reported a top-down approach to synthesize porous CdO by decomposition of $CdCO_3$ crystals.[39]

In this paper, uniform cobalt carbonate crystals with different shapes have been synthesized in high yield by a hydrothermal approach through tuning the volume ratio of a mixed solvent composed of water and ethanol (or glycerol). Calciniation of the $CoCO_3$ crystals results in the formation of nanoporous Co_3O_4 particles. The sensing property of the porous Co_3O_4 crystals has been examined.

2. Experimental Section

2.1. Materials and Preparation Procedures. All reagents were of analytical grade and were purchased and used as received without further purification. In a typical procedure, 1 mmol (0.2490 g) of cobalt acetate $[Co(CH_3COO)_2 \cdot 4H_2O]$ and 3.95×10^{-2} mmol (0.0144 g) of cetyltrimethylammonium bromide (CTAB) were dissolved in a 24 mL mixture of distilled water and ethanol (or glycerol) with different volume ratios in a Teflon liner (capacity of 30 mL) with a magnetic stirrer at room temperature. Then, 5 mmol (0.3950 g) of NH_4HCO_3 was added to the solution described above and stirred for 10 min. Finally, the liner was sealed in a stainless steel autoclave. The autoclave was maintained at 160 °C for 24 h and then cooled to room temperature naturally. The obtained pink-colored products were centrifuged, washed several times with distilled water and anhydrous ethanol, and dried at 60 °C. The thermal decomposition of the pink-colored precursor to Co_3O_4 was performed at 500 °C for 3 h in air in the oven.

2.2. Characterization. X-ray powder diffraction (XRD) patterns of the products were obtained on a Japan Rigaku DMax-γA rotation anode X-ray diffractometer equipped with graphite monochromatized Cu Kα radiation ($\lambda = 1.54178$ Å). The SEM images were taken on a field emission scanning elecrton microscope (JEOL JSM-6700F, 15

* To whom correspondence should be addressed. Fax: + 86 551 3603040. E-mail: shyu@ustc.edu.cn.

10.1021/cg8003068 CCC: $40.75
Published on Web 11/20/2008

Scheme 1. Illustration of the Working Principle of the Gas Sensing Measurement

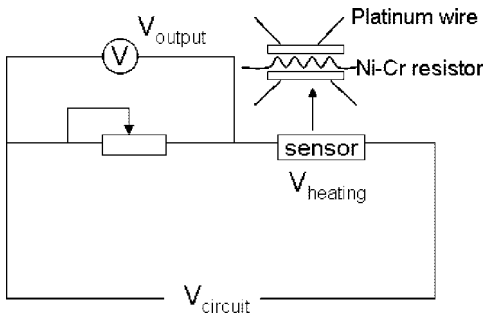

kV). FT-IR spectra were recorded on a Bruker Vector-22 FT-IR spectrometer from 4000 to 400 cm^{-1} at room temperature. The composition of the samples was analyzed with an X-ray photoelectron spectroscopy (XPS) technique, which was conducted on an ESCALAB 250 (Thermo Electron Corp.). The thermogravimetric analysis (TGA) measurement was carried out on a Diamond TG/DTA thermal analyzer (Perkin-Elmer) with a heating rate of 10 K min^{-1} in air. Brunauer−Emmett−Teller (BET) surface area measurement was performed on a Micromeritics ASAP-2000 nitrogen adsorption apparatus.

2.3. Experimental Procedure for Sensing Performance Measurement. Alcohol-sensing measurement was carried out on a home-built apparatus reported previously.[40c] The thick film sensors were made by depositing the thick films of Co_3O_4 particles on ceramic substrates with the connection through gold electrodes connected by four platinum wires. After calcination in air at 500 °C for 3 h, the platinum wires were connected with the leads of the gold electrodes to the instruments for gas sensing measurements. Then, the Ni−Cr−alloy coil used as the resistor was passed through the ceramic tubes and was attached to the electrode. Finally, the prepared sensors were fixed into the gas sensing apparatus (Scheme 1). During the measurement, the $V_{circuit}$ was applied to a certain value, and the heating voltage was used to heat the sensor. The detected output voltage of the load resistor connected with the sensor reflected the resistance change of the sensor, due to the various types and concentrations of the sensing gas. The higher value of the output voltage implied a lower resistance value and a better sensitivity of the sensor. The sensors were sealed into a bottle, and a given amount of ethanol was injected into the heating device part of apparatus with a microinjector and gasified quickly. The measurement data were collected through the computer.

3. Results and Discussion

3.1. Shape Control of Cobalt Carbonate Microcrystals in a Water/Ethanol Solvent. The phases of the as-prepared pink-colored samples obtained in pure water or ethanol solution were examined by the XRD patterns as shown in Figure 1. The intensities of the sharp diffraction peaks indicated that the product has good crystallinity. All of the diffraction peaks in the XRD patterns can be indexed as a pure hexagonal phase of $CoCO_3$ with the following cell constants: $a = 4.661$ Å, and $c = 14.96$ Å (JCPDS card 78-0209).

A mixture of the irregular and nearly spherical microspheres <10 μm in size and a small fraction of bigger crystals were observed by a general overview SEM image shown in Figure 2a. The high-magnification SEM image in Figure 2b revealed two types of main morphologies of the as-prepared $CoCO_3$ crystals, i.e., the agglomerates of the cuboids piled together and the microspheres with a mean diameter of 5 μm composed of the small cuboids. All the smaller cuboids have smooth surfaces. The SEM image in Figure 2c indicates that the $CoCO_3$ crystals prepared in a pure ethanol solution exhibit jujube-like morphologies. A high-magnification SEM image revealed that each of the jujube-like crystals with an average size of 3.5 μm is composed of irregular blocks.

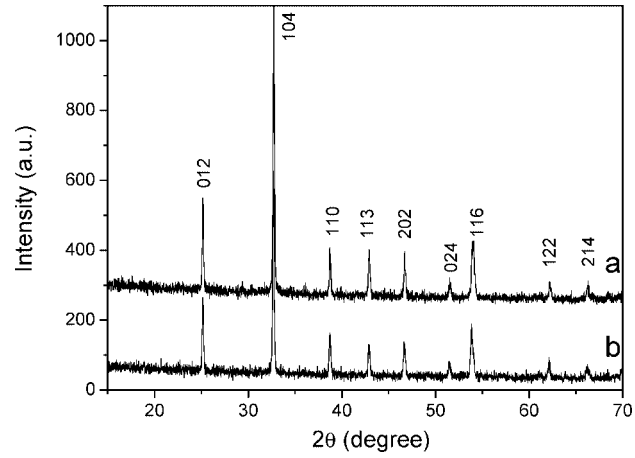

Figure 1. XRD patterns of the pink-colored crystals obtained in (a) an aqueous solution and (b) an alcohol solution.

According to the analyses described above, the morphology and the microstructure of the as-prepared crystals can be changed by altering the solvents used. However, uniform particles cannot be obtained in pure water or pure ethanol. However, a series of samples with different shapes and structures can be synthesized by altering the volume ratios of water and ethanol in a mixed solvent. The XRD patterns of the as-prepared samples formed in the different volume ratios of water/ethanol solutions showed that the hexagonal $CoCO_3$ phase formed as indicated from the sharpening diffraction peaks (Figure 3).

The FT-IR spectrum further revealed the composition of pink-colored crystals formed in the different volume ratios of water/ethanol solvents (see Figure S1a of the Supporting Information), taking the sample prepared with volume ratio of water and ethanol of 1:1, for example. The bands at 1421, 1115, and 867 cm^{-1} were assigned to the different vibrational modes of the carbonate anions of the $CoCO_3$ crystal.[41−43]

Further evidence of the purity and composition of the samples obtained from the solution with a volume ratio of water to ethanol of 1:1 was collected via X-ray photoelectron spectroscopy (XPS). The sharp peaks at 284.8, 531.8, and 782.4 eV in Figure 4a correspond to the characteristic peaks of C1s, O1s, and Co2p, respectively, indicating the existence of carbon, oxygen, and cobalt elements in the sample, respectively. The peak at 288.8 eV in the C1s core spectrum of Figure 4b shows that the carbon is combined with oxygen in the carbonate ions of the crystals. Thus, on the basis of all the results mentioned above, it is clear that the composition of the crystals synthesized from the water/ethanol solutions is cobalt carbonate.

The SEM images in Figure 5 show the morphologies and structures of the $CoCO_3$ crystals obtained from the mixed solutions with different volume ratios of water to ethanol. When the volume ratio of water to ethanol was 1:1, uniform $CoCO_3$ microspheres were obtained (Figure 5a). Further examination of the SEM image of the obtained microspheres in the inset of Figure 5a reveals that plenty of the uniform cuboids piled up together tightly to form microspheres with an average diameter of 4 μm. The higher magnification of the SEM image in Figure 5b shows the smooth surface of each regular cuboid. The microspheres $\sim$4.5 μm in size were composed of irregular cuboids with a mean length of 1.5 μm as indicated from the SEM image of Figure 5c when the volume ratio of water to ethanol became 1:2. Moreover, these cuboids were not aligned in order, taking an out-of-order way to assemble together to form the microspheres. Further decreasing the volume ratio of

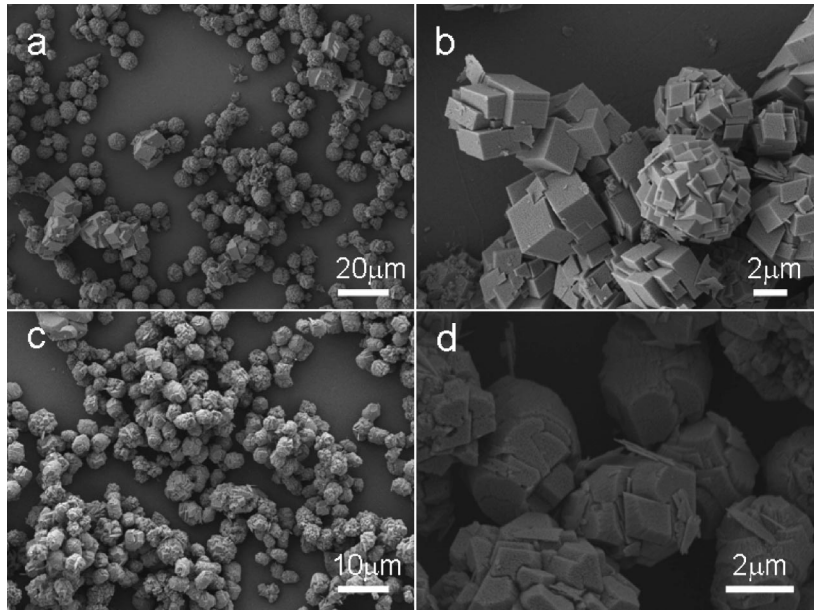

Figure 2. Low- and high-magnification SEM images of $CoCO_3$ crystals prepared in different media: (a and b) pure water and (c and d) ethanol.

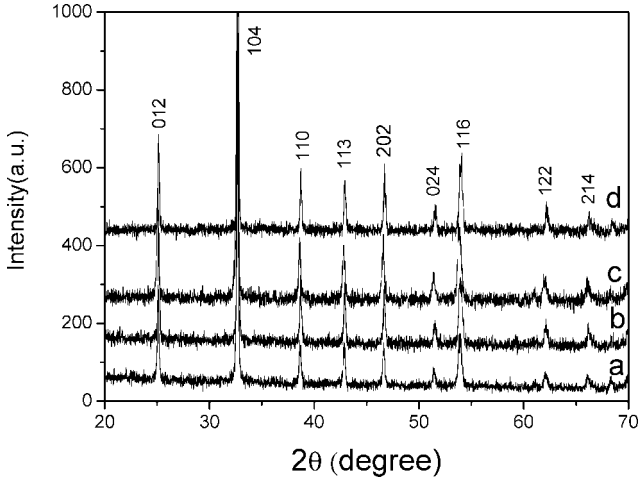

Figure 3. XRD patterns of $CoCO_3$ crystals with novel microstructures formed in water/ethanol solutions with volume ratios of (a) 1:1, (b) 1:3, (c) 1:5, and (d) 1:7.

water to ethanol to 1:3 resulted in the aggregates with the pores in the center shown from the image of Figure 5d. The particles assembled into aggregates were changed from cuboids to irregular polyhedrons hundreds of nanometers in mean size by further decreasing the volume ratio of water to ethanol. Figure 5e shows the SEM image of the aggregates with an average length of 2.5 μm obtained from the solution with a volume ratio of 1:5. The inset SEM image reveals the detail morphologies and structures of the crystals, showing that the aggregates formed by stacking of the smooth flakes 400 nm in mean size. When the volume ratio of water to ethanol was further decreased to 1:7, the flowerlike $CoCO_3$ crystals with a diameter of 4 μm were prepared as shown in Figure 5f.

The SEM images of panels g and h of Figure 5 show the morphologies of the crystals when the volume ratio of water to ethanol is further decreased to 1:11 and 1:15, respectively. A large quantity of spheres composed of small particles assembled together, and a few flakelike substances with a mean diameter 2 μm appeared in the SEM images compared with the high volume ratio of water to ethanol. The XRD patterns (Supporting Information Figure S2) of the reveal the compositions of the obtained samples prepared at volume ratios of water to ethanol of 1:11 and 1:15. The diffraction peaks marked with an asterisk in the XRD patterns can be indexed as a monoclinic phase of $Co_2(CO_3)(OH)_2$ with cell constants $a = 9.368$ Å, $b = 12.07$ Å, and $c = 3.389$ Å (JCPDS card 29-1416) and other diffraction peaks assigned to hexagonal phase of $CoCO_3$ with cell constants $a = 4.661$ Å and $c = 14.96$ Å (JCPDS card 78-0209). The flakelike crystals were similar in morphology to the reported leaves of the roselike architectures and belonged to the $Co_2(CO_3)(OH)_2$ phase.[44]

The effects of the concentration of CTAB on the morphology and structure of the $CoCO_3$ crystals have been investigated. The microspheres with a size of 5 μm, which are composed of cuboids, were obtained in a mixed solution with a volume ratio of 1:1 (water/ethanol) in the absence of CTAB (see Figure S3a of the Supporting Information). However, both the cuboids with an average edge length of 2 μm and the microspheres became larger compared with those in Figure 5b. Furthermore, the cuboids were not aligned regularly to build up the microspheres but were stacked together randomly. The results indicated that CTAB played an important role in controlling the size of the crystals and in the arrangement of the composed building blocks. If the amount of CTAB was increased to 0.8 mmol, equal to 20 times the amount of CTAB used in the sample shown in Figure 5b, a single phase of pink-colored $CoCO_3$ crystals was still obtained. However, the cuboids and the quasi-spherical spheres became much more irregular (see Figure S3b of the Supporting Information). These analyses indicated that not only the existence of CTAB but also the amount of CTAB has a significant influence on the formation of the uniform microspheres with novel structures.

The growth and nucleation mechanism of the $CoCO_3$ microsphere with uniform cuboids formed in a water/ethanol solution with a volume ratio of 1:1 can be explained by a dissolution−renucleation process[37,45] and aggregation-based mechanism.[16b,17a,20,45] When the reagents were added into the reaction system completely at room temperature, a large amount of amorphous particles precipitated with no apparent diffraction peaks in the

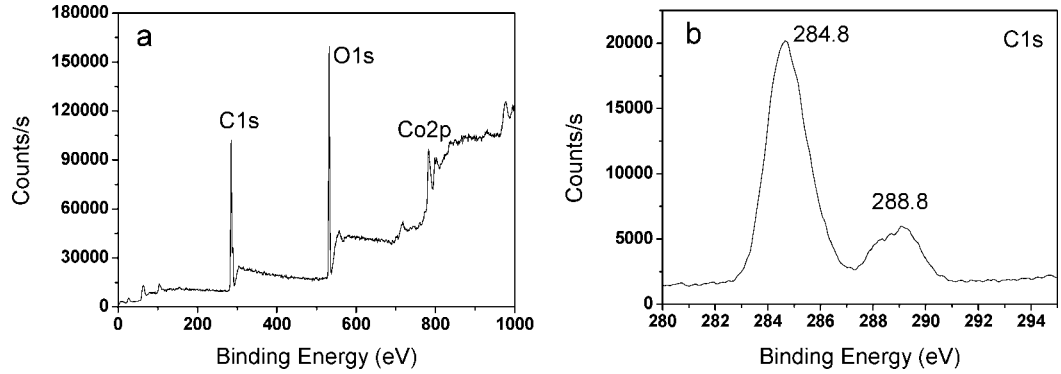

Figure 4. (a) XPS survey spectrum of the $CoCO_3$ crystals formed in a water/ethanol solution with a volume ratio of 1:1. (b) High-resolution XPS spectrum of C1s.

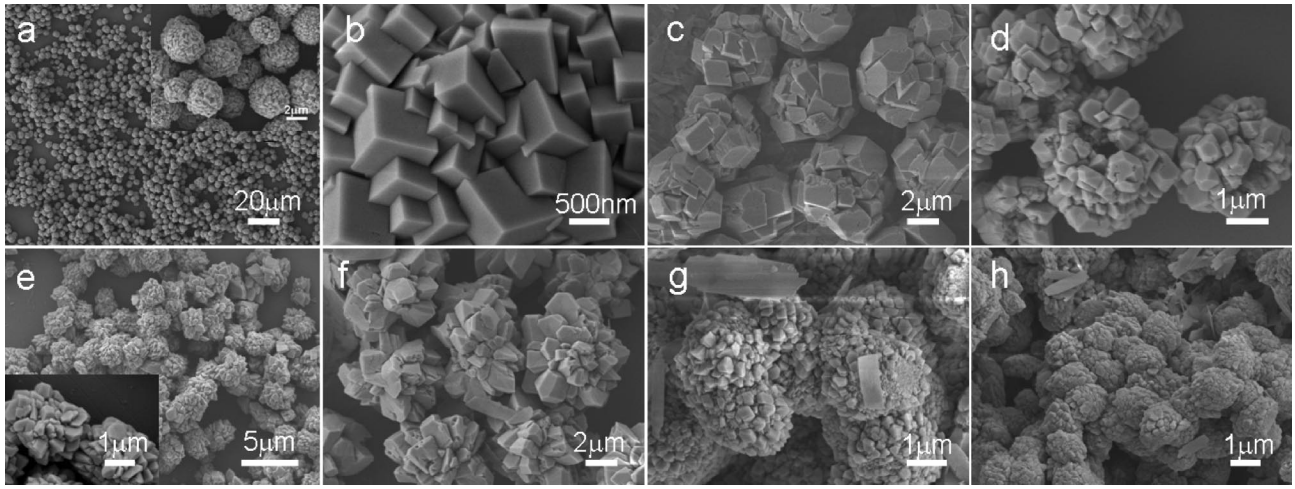

Figure 5. (a) SEM image of the $CoCO_3$ crystals formed in the water/ethanol mixture at a volume ratio of 1:1 (inset showing a high-magnification SEM picture). (b) Magnified image of a microsphere in panel a, showing the smooth surface of the cuboid. (c−h) SEM images of the $CoCO_3$ crystals formed in the water/ethanol mixture at volume ratios of (c) 1:2, (d) 1:3, (e) 1:5 (inset showing a high-magnification SEM picture), (f) 1:7, (g) 1:11, and (h) 1:15.

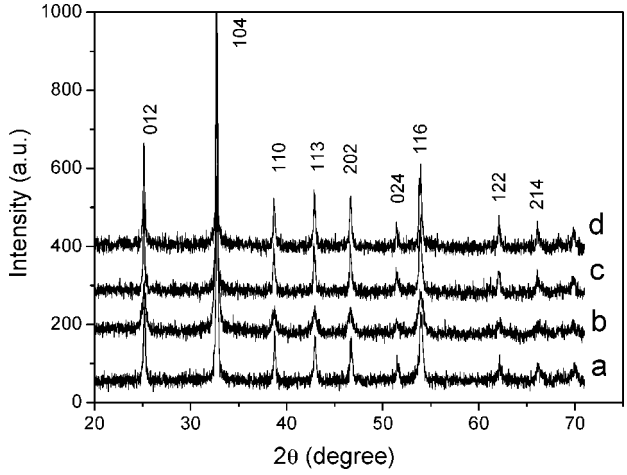

Figure 6. XRD patterns of $CoCO_3$ crystals with novel microstructures formed in a water/glycerol mixed solution with different volume ratios of (a) 1:1, (b) 1:3, (c) 1:5, and (d) 1:11.

XRD pattern. Such an initial supersaturated amorphous phase resulted in a fast nucleation at the initial stage. After nucleation, this unstable phase grew and transformed into the stable particles by a dissolution−renucleation process. When these precursors formed and stopped growing, these small cuboids aggregated together under the influence of the electrostatic multipole field[46] by an aggregation-based mechanism and grew into the $CoCO_3$ microsphere with uniform cuboids finally. The microspheres were so firm that a 2 h strong sonication was needed to break them up into small individual cuboids (see Figure S4 of the Supporting Information).

According to the experimental results, the volume ratio of water to ethanol has a significant influence on the final morphology and structure of the $CoCO_3$ crystals. With a decrease in the content of water in a mixed solvent, the polarity of the solution decreases and the solubility of the reactant decreases similarly. Thus, the rate of nucleation of the crystal is increased, which results in an increase in the particle number.[47] However, the H_2O molecule is quite small and can be easily polarized, which can effectively stabilize the ions in the solution, especially anions, in a hydrogen-bond type, leading to the low reactivity of the reactant.[48] Thus, the reactivity of the ions in the solution increases followed by an increase in the content of ethanol in the mixed solvent. With a higher ethanol content, the number of nucleation particles is larger and the reactivity of the reactant is higher, and then the reaction rate is faster, which results in there being a lack of time to age and aggregate the particles in order and to produce the crystals with irregular morphologies, finally.

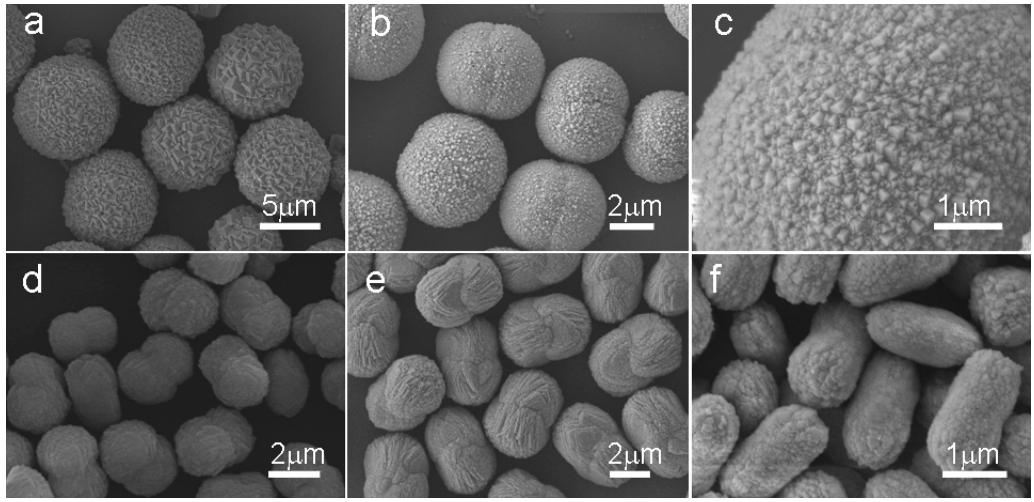

Figure 7. SEM images of the $CoCO_3$ crystals formed in a mixed solvent of water and glycerol with volume ratios of (a) 1:1, (b and c) 1:3, (d) 1:5, (e) 1:11, and (f) 1:15.

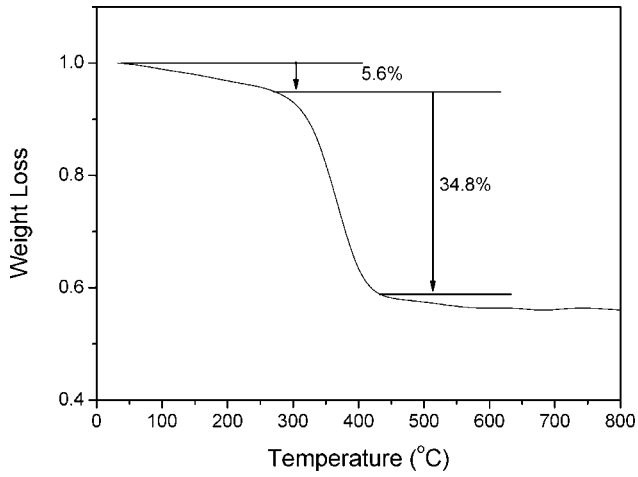

Figure 8. TGA curve of the $CoCO_3$ crystals formed in a mixed solvent of water and ethanol with a volume ratio of 1:1.

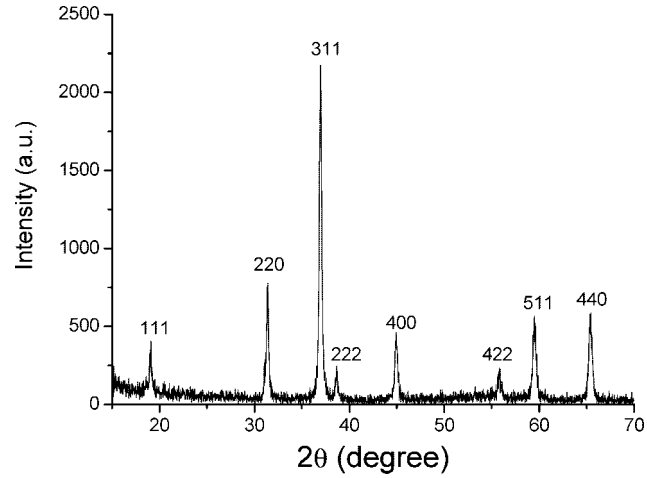

Figure 9. XRD patterns of Co_3O_4 particles by calcination of $CoCO_3$ particles at 500 °C, which were prepared in a mixed solvent of water and ethanol with a volume ratio of 1:1.

3.2. Shape Control of Cobalt Carbonate Microcrystals in a Water/Glycerol Solvent. The XRD patterns were performed on the samples prepared from the mixed solvent of water and glycerol with different volume ratios to identify the phases. Figure 6 shows the similar XRD patterns of these samples, which revealed a pure hexagonal phase of $CoCO_3$ with cell constants $a = 4.661$ Å and $c = 14.96$ Å from the sharp diffraction peaks. Figure 7 shows the SEM images of a series of samples prepared in a mixed solvent of water and glycerol with different volume ratios. When the volume ratio of water and glycerol was 1:1, uniform pink-colored $CoCO_3$ microspheres 6 μm in size were produced in Figure 7a, the surfaces of which were composed of smaller regular tetrahedra for comparison with the crystals prepared from the mixed solvent of water and ethanol with a volume ratio of 1:1 (shown in Figure 5a). With a decrease in the volume ratio of water to glycerol to 1:3, the microspheres were elongated to coupled twin-shaped hemispheres with length of 4 μm as revealed in the SEM image of Figure 7b. The surfaces of these uniformly coupled hemispheres were not smooth, composed of smaller tetrahedra tens of nanometers in average size as indicated from the magnified SEM image of Figure 7c. When the volume ratio of water to glycerol was decreased to 1:5 (Figure 7d), the trend of the split of the coupled hemispheres became clear and formed the dumbbell-like $CoCO_3$ crystals 3 μm in length. The dumbbell-like $CoCO_3$ evolved into peanut-shaped crystals with a length of 3 μm followed by a decrease in the volume ratio of water to glycerol of 1:11 (Figure 7e). The $CoCO_3$ peanutlike particles in a form of layered structure have a rather smooth surface. With a further decrease in the volume ratio of water to glycerol to 1:15, the $CoCO_3$ microrods with a length of 1.5 μm were obtained as revealed by the SEM image in Figure 7f.

The transition process of a series of $CoCO_3$ crystals formed in the mixed solvent of water and glycerol with different volume ratios is consistent with the so-called "rod−dumbbell−sphere" morphogenesis mechanism, a universal growth process directed by the intrinsic electric fields in the mineralization of metal carbonates[16b,17a] and fluoroapatite.[49] However, the rod−dumbbell−sphere morphology transition of the $CoCO_3$ crystals is not based on the time-dependent evolution process, but on changing the volume ratio of the water to glycerol in solution. With an increase in the volume ratio of water to glycerol from 1:15 to 1:1, the polarity of the solvent is gradually increased, the reactivity of ions in the solution decreases, and the reaction rate of the reactants decreases. Thus, the change in the composition of a mixed solvent has a significant influence on the shape of the $CoCO_3$ crystals.

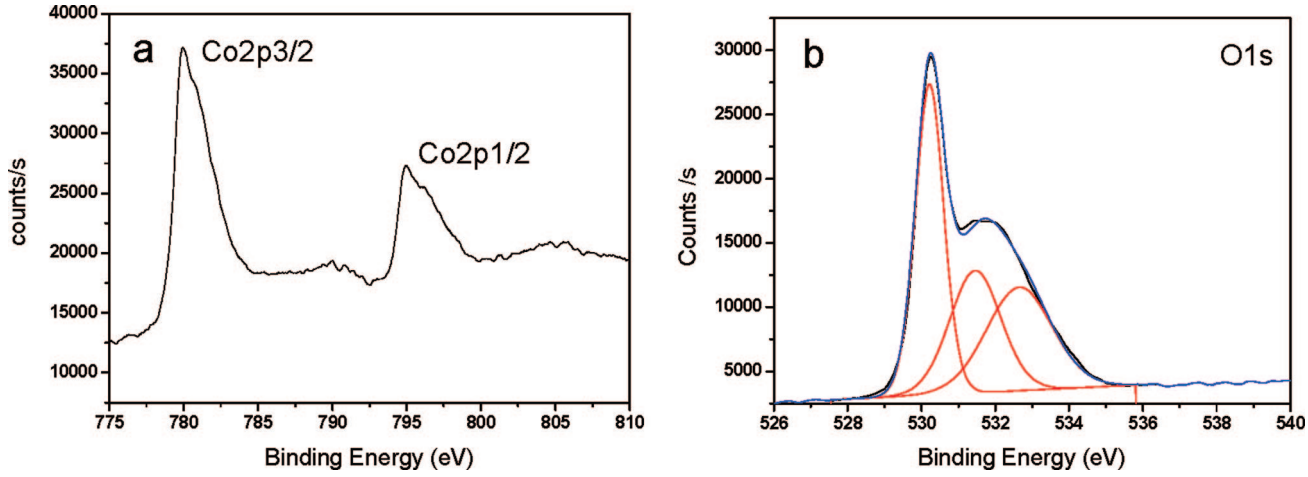

Figure 10. High-resolution XPS spectra of (a) Co2p and (b) O1s in the Co_3O_4 particles prepared by calcination of the $CoCO_3$ precursor synthesized from a mixed solvent of water and ethanol with a volume ratio of 1:1.

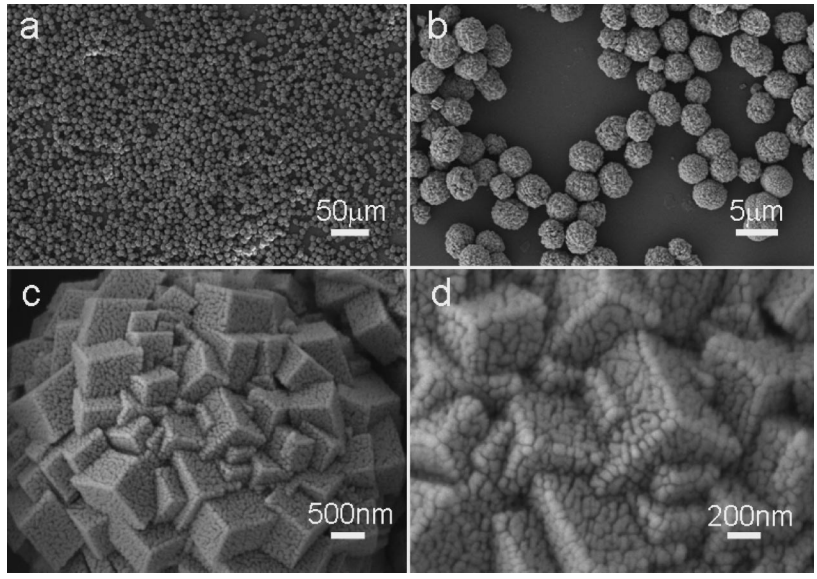

Figure 11. SEM images of the nanoporous Co_3O_4 particles produced by calcination of the spherical $CoCO_3$ particles at 500 °C, which were prepared in a mixed solvent of water and ethanol with a volume ratio of 1:1.

3.3. Preparation of Nanoporous Co_3O_4 Particles. The thermal stability of the $CoCO_3$ crystals formed in a mixed solvent of water and ethanol with a volume ratio of 1:1 has been investigated by TGA analysis (Figure 8). The gradual mass loss of 5.6 wt % at ~200 °C was mainly due to the evaporation of absorbed water or surfactants attached to the surface of the microsphere. A well-defined decrease in the dominant weight loss profile at ~400 °C was 34.8 wt %, which can be attributed to the decomposition of $CoCO_3$ to Co_3O_4 in the atmosphere (the second stage of weight loss shown in Figure 8). On the basis of the TGA results, the temperature for the calcination of the $CoCO_3$ precursor to Co_3O_4 particles was set at 500 °C for 3 h to ensure the complete decomposition of the $CoCO_3$ precursor.

The XRD pattern in Figure 9 confirms that the product obtained by calcination of the $CoCO_3$ precursor synthesized in a mixed solvent of water and ethanol with a volume ratio of 1:1 can be indexed as a cubic phase Co_3O_4 with a space group of *Fd3m* (JCPDS card 78-1970). The sharp bands at 664 and 573 cm^{-1} in the FTIR spectrum are the characteristic vibration peaks of the Co−O mode,[50] evidence of the phase of Co_3O_4

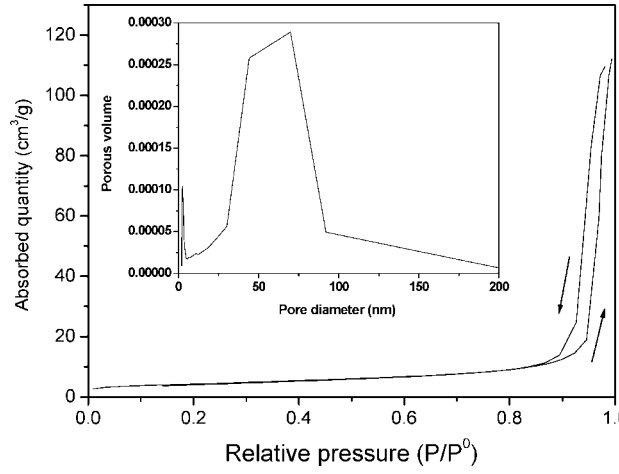

Figure 12. N_2 adsorption−desorption isothermal curve of the calcinated Co_3O_4 microspheres. The inset shows the corresponding pore size distribution.

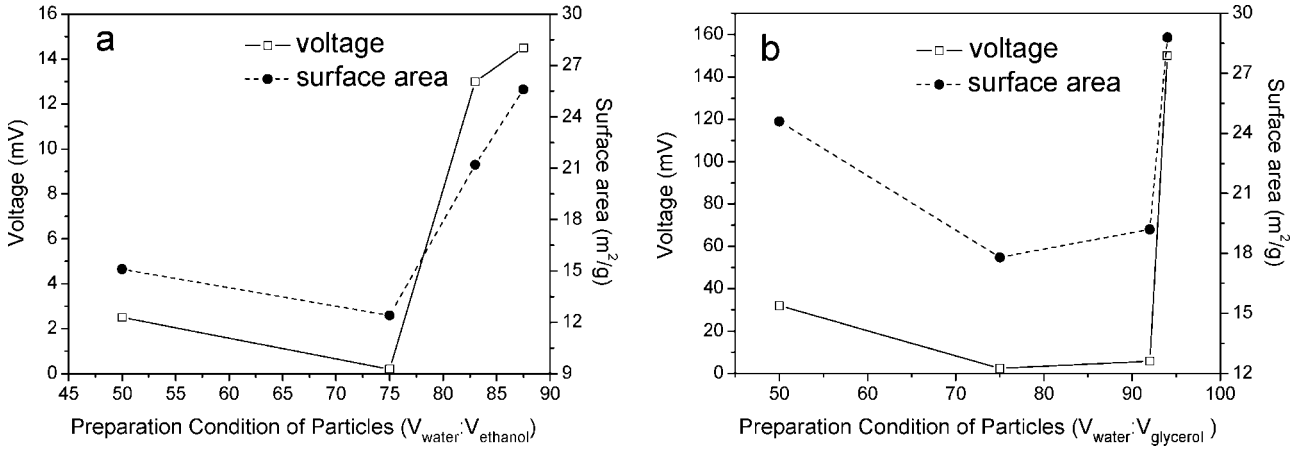

Figure 13. Changes in voltage to 50 ppm alcohol at 300 °C (□, solid line) and BET surface area (●, dashed line) for the Co_3O_4-based sensor as a function of the different Co_3O_4 particles prepared from the mixed solvents of (a) water and ethanol and (b) water and glycerol.

(see Figure S1b of the Supporting Information). The XPS spectra provide firm proof of the composition of the calcinated product from the $CoCO_3$ precursor. Figure 10 shows that the two core level peaks at 780.2 and 795.3 eV correspond to Co2p3/2 and Co2p1/2 of Co_3O_4, respectively.[51] The three peaks in the O1s core spectrum at 530.2, 531.5, and 532.8 eV can be indexed as gaseous oxygen, O^{2-} combined with Co^{2+}, and Co^{3+}, respectively.[44]

After calcination of the $CoCO_3$ precursor at 500 °C, no noticeable shape change was observed. SEM images in Figure 11a,b indicate that the Co_3O_4 particles calcinated from the $CoCO_3$ particles formed in a mixed solvent of water and ethanol with a volume ratio of 1:1 still preserved their uniformly spherical shape and have an average diameter of 2.5 μm. However, the surfaces of Co_3O_4 microspheres became rough after calcination. The detailed observation indicated that all particles have nanopores and each cuboid became porous (Figure 11c,d). The formation of the nanoporous cobalt oxide architectures can be attributed to the release of carbon dioxide from the cobalt carbonate crystals from different directions.[39]

The porous structures of the calcinated Co_3O_4 microspheres were further revealed by the N_2 adsorption−desorption isothermal curve in Figure 12. The BET surface area of the microspheres was 15.1 m^2/g, and the pore size distribution curve in the inset exhibited bimodal pore distributions. The pores at ~2.5 and 60 nm originated from the surface pore formed by the release of CO_2 and the gaps between two cuboids, respectively, which can be confirmed directly by the SEM observation (Figure 11c,d).

3.4. Sensing Performance of Nanoporous Co_3O_4 Particles. The 50 ppm alcohol-sensing performances of the nanoporous Co_3O_4 particles synthesized from the precursors obtained from different mixed solvents have been presented as dynamic response curves (see Figure S5 of the Supporting Information). We found that these sensors exhibit good reversibility as revealed from the stable fifty-fold on−off responses for the porous Co_3O_4 particles without obvious changes in the observed signals. The zero output voltage signal value in the "on-response" stage and the short response time reveal the non-sensing to the air of the particles and the fast, sensitive response to the alcohol.[52] The plots in Figure 13 show the relationship of the voltage and the BET surface area with respect to the Co_3O_4 samples prepared under different conditions, according to the voltage values of dynamic response curves of the samples. It can be seen that the signal voltage of the cobalt oxide increased with the increase in surface area of the particles prepared from either the water/ethanol or water/glycerol solvent. In the water/ethanol preparation system, when the volume ratio of water to ethanol is 1:7, the higher voltage value (14.5 mV) corresponds to the larger BET surface area (25.6 m^2/g). In the same way, the voltage (150 mV) and the BET surface area (28.8 m^2/g) are the highest values for the sample synthesized from a mixed solvent of water and glycerol with a volume ratio of 1:15, which means the highest sensitivity among the particles in the water/glycerol preparation condition, due to the nanoporous structure and smallest size of particles (shown in the SEM image of Figure 7f) with the largest surface area. Thus, it is noticeable that the sensitivity of the semiconductor is proportional to the BET surface area of the particles prepared from the same kind of mixed solvent system.

The change of voltage in sensors is mainly attributed to the adsorption and desorption of the gas molecules of the surface conductivity modulation.[37,40] The higher surface area can result in a larger fraction of the atoms presented at the surface, which permits more gas molecules to enter and approach the active position easily. Thus, the sensitive response and good reversibility of the porous Co_3O_4 particles described here can be caused by the large surface area and the pores with uniform sizes, which favor greater exposure of the surfaces to the gas molecules more effectively.

4. Conclusions

In summary, cobalt carbonate crystals with novel structures and morphologies can be synthesized by a hydrothermal process in a water/ethanol (or water/glycerol) mixed solution by tuning the volume ratio of the solvents. Nanoporous cobalt oxide particles can be produced by calcination of the $CoCO_3$ precursors and preserve the original shape of the precursor crystals. The nanoporous Co_3O_4 particles exhibit sensitive response and reversibility in sensing performance. The combination of a solution mineralization reaction with a traditional thermal decomposition process allows us to synthesize other nanoporous oxide materials with novel architectures.

Acknowledgment. This work was supported by the National Science Foundation of China (Grants 50732006, 20701035, 20621061, and 20671085), 2005CB623601, the Anhui Development Fund for Talent Personnel and Anhui Education Committee (2006Z027 and ZD2007004-1), the Specialized Research Fund for the Doctoral Program (SRFDP) of Higher Education

State Education Ministry, and the Partner-Group of the Chinese Academy of Sciences-the Max Planck Society.

Supporting Information Available: FT-IR spectra, XRD patterns, SEM images of the $CoCO_3$ crystals synthesized from the mixed solvent, and dynamic response curves for the Co_3O_4-based sensor. This material is available free of charge via the Internet at http://pubs.acs.org.

References

(1) (a) Park, W. I.; Yi, G. C. *Adv. Mater.* **2004**, *16*, 87. (b) Baxter, J. B.; Aydil, E. S. *Appl. Phys. Lett.* **2005**, *86*, 053114. (c) Tseng, Y. K.; Huang, C. J.; Cheng, H. M.; Lin, I. N.; Liu, K. S.; Chen, I. C. *Adv. Funct. Mater.* **2003**, *13*, 811.

(2) (a) Templeton, A. C.; Wuelfing, W. P.; Murray, R. W. *Acc. Chem. Res.* **2000**, *33*, 27. (b) Elghanian, R.; Storhoff, J. J.; Mucic, R. C.; Letsinger, R. L.; Mirkin, C. A. *Science* **1997**, *277*, 1078. (c) Daniel, M. C.; Astruc, D. *Chem. Rev.* **2004**, *104*, 293.

(3) (a) Wu, J. J.; Lee, Y. L.; Chiang, H. H.; Wong, D. K. P. *J. Phys. Chem. B* **2006**, *110*, 18108. (b) Huo, L.; Li, W.; Lu, L.; Cui, H.; Xi, S.; Wang, J.; Zhao, B.; Shen, Y.; Lu, Z. *Chem. Mater.* **2000**, *12*, 790. (c) Amin, N.; Arajs, S. *Phys. Rev. B* **1987**, *35*, 4810.

(4) (a) Burda, C.; Chen, X.; Narayanan, R.; El-Sayed, M. A. *Chem. Rev.* **2005**, *105*, 1025. (b) Peng, X. G.; Manna, L.; Yang, W. D.; Wickham, J.; Scher, E.; Kadavanich, A.; Alivisatos, A. P. *Nature* **2000**, *404*, 59. (c) Yu, W. W.; Peng, X. G. *Angew. Chem., Int. Ed.* **2002**, *41*, 2368.

(5) (a) Li, H.; Liu, R.; Zhao, R. X.; Zheng, Y. F.; Chen, W. X.; Xu, Z. D. *Cryst. Growth Des.* **2006**, *6*, 2795. (b) Switzer, J. A.; Kothari, H. M.; Bohannan, E. W. *J. Phys. Chem. B* **2002**, *106*, 4027. (c) Siegfried, M. J.; Choi, K. S. *Angew. Chem., Int. Ed.* **2005**, *44*, 3218.

(6) (a) Yao, W. T.; Yu, S. H.; Wu, Q. S. *Adv. Funct. Mater.* **2007**, *17*, 623. (b) Qian, H. S.; Yu, S. H.; Gong, J. Y.; Luo, L. B.; Fei, L. F. *Langmuir* **2006**, *22*, 3830. (c) Cui, X. J.; Yu, S. H.; Li, L. L.; Li, K.; Yu, B. *Adv. Mater.* **2004**, *16*, 1109.

(7) (a) Wang, C.; Hou, Y. L.; Kim, J. M.; Sun, S. H. *Angew. Chem., Int. Ed.* **2007**, *46*, 6333. (b) Zhang, Q.; Chen, X. Y.; Zhou, Y. X.; Zhang, G. B.; Yu, S. H. *J. Phys. Chem. C* **2007**, *111*, 3927. (c) Sreeprasad, T. S.; Samal, A. K.; Pradeep, T. *Langmuir* **2007**, *23*, 9463.

(8) (a) Zheng, S. F.; Hu, J. S.; Zhong, L. S.; Wan, L. J.; Song, W. G. *J. Phys. Chem. C* **2007**, *111*, 11174. (b) Bachmann, J.; Jing, J.; Knez, M.; Barth, S.; Shen, H.; Mathur, S.; Gosele, U.; Nielsch, K. *J. Am. Chem. Soc.* **2007**, *129*, 9554.

(9) (a) Zhang, L.; Ruh, E.; Grutzmacher, D.; Dong, L. X.; Bell, D. J.; Nelson, B. J.; Schonenberger, C. *Nano Lett.* **2006**, *6*, 1311. (b) Fang, X. S.; Ye, C. H.; Zhang, L. D.; Xie, T. *Adv. Mater.* **2005**, *17*, 1661. (c) Song, R. Q.; Xu, A. W.; Yu, S. H. *J. Am. Chem. Soc.* **2007**, *129*, 4152.

(10) (a) Xu, L. Q.; Zhan, J. H.; Hu, J. Q.; Bando, Y.; Yuan, X. L.; Sekiguchi, T.; Mitome, M.; Golberg, D. *Adv. Mater.* **2007**, *19*, 2141. (b) Wang, X.; Li, L.; Zhang, Y. G.; Wang, S. T.; Zhang, Z. D.; Fei, L. F.; Qian, Y. T. *Cryst. Growth Des.* **2006**, *6*, 2163. (c) Sun, Y. A.; Xia, Y. N. *Adv. Mater.* **2003**, *15*, 695.

(11) (a) Paek, J.; Lee, C. H.; Choi, J.; Choi, S. Y.; Kim, A.; Lee, J. W.; Lee, K. *Cryst. Growth Des.* **2007**, *7*, 1378. (b) Cho, K. S.; Talapin, D. V.; Gaschler, W.; Murray, C. B. *J. Am. Chem. Soc.* **2005**, *127*, 7140. (c) Yada, M.; Sakai, S.; Torikai, T.; Watari, T.; Furuta, S.; Katsuki, H. *Adv. Mater.* **2004**, *16*, 1222.

(12) (a) Hou, Y. L.; Xu, Z. C.; Sun, S. H. *Angew. Chem., Int. Ed.* **2007**, *46*, 6329. (b) Jesson, D. A.; Abel, M. L.; Hay, J. N.; Smith, P. A.; Watts, J. F. *Langmuir* **2006**, *22*, 5144. (c) Selvakannan, P. R.; Sastry, M. *Chem. Commun.* **2005**, *13*, 1684.

(13) (a) Yan, H.; He, R.; Pham, J.; Yang, P. *Adv. Mater.* **2003**, *15*, 403. (b) Zhang, H.; Yang, D.; Ji, Y. J.; Ma, X. Y.; Xu, J.; Que, D. L. *J. Phys. Chem. B* **2004**, *108*, 3955.

(14) Dalas, E.; Klepetsanis, P.; Koutsoukos, P. G. *Langmuir* **1999**, *15*, 8322.

(15) Cölfen, H. *Curr. Opin. Colloid Interface Sci.* **2003**, *8*, 23.

(16) (a) Yu, S. H.; Cölfen, H.; Tauer, K.; Antonietti, M. *Nat. Mater.* **2005**, *4*, 51. (b) Yu, S. H.; Cölfen, H.; Xu, A. W.; Dong, W. F. *Cryst. Growth Des.* **2004**, *4*, 33.

(17) (a) Yu, S. H.; Cölfen, H.; Antonietti, M. *J. Phys. Chem. B* **2003**, *107*, 7396. (b) Wang, C. M.; Cheng, Y.; Wang, Y. S.; Bao, F. *Chin. J. Struct. Chem.* **2007**, *26*, 757.

(18) (a) Wu, X. L.; Cao, M. H.; Lu, H. Y.; He, X. Y.; Hu, C. W. *J. Nanosci. Nanotechnol.* **2006**, *6*, 2123. (b) Wang, X.; Li, Y. D. *Mater. Chem. Phys.* **2003**, *82*, 419.

(19) (a) Manoli, F.; Dalas, E. *J. Cryst. Growth* **2000**, *218*, 359. (b) Qi, L. M.; Ma, J. M. *Gaodeng Xuexiao Huaxue Xuebao* **2002**, *23*, 1595.

(20) Guo, X. H.; Yu, S. H.; Cai, G. B. *Angew. Chem., Int. Ed.* **2006**, *45*, 3977.

(21) Guo, X. H.; Xu, A. W.; Yu, S. H. *Cryst. Growth Des.* **2008**, *8*, 1233.

(22) Xiao, J.; Wang, J. F.; Liu, Y. D.; Li, J.; Liu, Y. X. *Zhongnan Gongye Daxue Xuebao* **2006**, *13*, 642.

(23) (a) Choi, S. D.; Min, B. K. *Sens. Actuators, B* **2001**, *77*, 330. (b) Wollenstein, J.; Burgmair, M.; Plescher, G.; Sulima, T.; Hildenbrand, J.; Bottner, H.; Eisele, I. *Sens. Actuators, B* **2003**, *93*, 442.

(24) (a) Jansson, J.; Palmqvist, A. E. C.; Fridell, E.; Skoglundh, M.; Österlund, L.; Thormählen, P.; Langer, V. *J. Catal.* **2002**, *211*, 387. (b) Fujita, S.; Suzuki, K.; Mori, T. *Catal. Lett.* **2003**, *86*, 139.

(25) Kang, Y. M.; Song, M. S.; Kim, J. H.; Kim, H. S.; Park, M. S.; Lee, J. Y.; Liu, K. H.; Dou, S. X. *Electrochim. Acta* **2005**, *50*, 3667.

(26) Da Fonseca, C. N. P.; De Paoli, M. A.; Gorenstein, A. *Sol. Energy Mater. Sol. Cells* **1994**, *33*, 73.

(27) (a) Takada, S.; Fujii, M.; Kohiki, S. *Nano Lett.* **2001**, *1*, 379. (b) Makhlouf, S. A. *J. Magn. Magn. Mater.* **2002**, *246*, 184.

(28) (a) Xu, R.; Zeng, H. C. *Langmuir* **2004**, *20*, 9780. (b) Xu, R.; Zeng, H. C. *J. Phys. Chem. B* **2003**, *107*, 926.

(29) Guan, H. Y.; Shao, C. L.; Wen, S. B.; Chen, B.; Gong, J.; Yang, X. H. *Mater. Chem. Phys.* **2003**, *82*, 1002.

(30) Shi, X. S.; Han, S.; Sanedrin, R. J.; Zhou, F.; Selke, M. *Chem. Mater.* **2002**, *14*, 1897.

(31) (a) Lakshmi, B. B.; Patrissi, C. J.; Martin, C. R. *Chem. Mater.* **1997**, *9*, 2544. (b) Liu, Y.; Wang, G.; Xu, C.; Wang, W. *Chem. Commun.* **2002**, 1486.

(32) Yu, T.; Zhu, Y. W.; Xu, X. J.; Shen, Z. X.; Chen, P.; Lim, C. T.; Thong, J. T. L.; Sow, C. H. *Adv. Mater.* **2005**, *17*, 1595.

(33) He, T.; Chen, D. R.; Jiao, X. L.; Wang, Y. L. *Adv. Mater.* **2006**, *18*, 1078.

(34) He, T.; Chen, D. R.; Jiao, X. L.; Xu, Y. Y.; Gu, Y. X. *Langmuir* **2004**, *20*, 8404.

(35) Rumplecker, A.; Kleitz, F.; Salabas, E.-L.; Schuth, F. *Chem. Mater.* **2007**, *19*, 485.

(36) (a) Hou, Y. L.; Kondoh, H.; Shimojo, M.; Kogure, T.; Ohta, T. *J. Phys. Chem. B* **2005**, *109*, 19094. (b) Yang, L. X.; Zhu, Y. J.; Li, L.; Zhang, L.; Tong, H.; Wang, W. W.; Cheng, G. F.; Zhu, J. F. *Eur. J. Inorg. Chem.* **2006**, 4787.

(37) Cao, A. M.; Hu, J. S.; Liang, H. P.; Song, W. G.; Wan, L. J.; He, X. L.; Gao, X. G.; Xia, S. H. *J. Phys. Chem. B* **2006**, *110*, 15858.

(38) Wang, Z. H.; Chen, X. Y.; Zhang, M.; Qian, Y. T. *Solid State Sci.* **2005**, *7*, 13.

(39) Yu, H. D.; Wang, D. S.; Han, M. Y. *J. Am. Chem. Soc.* **2007**, *129*, 2333.

(40) (a) Wang, Y. L.; Jiang, X. C.; Xia, Y. N. *J. Am. Chem. Soc.* **2003**, *125*, 16176. (b) Liu, J. F.; Wang, X.; Peng, Q.; Li, Y. D. *Adv. Mater.* **2005**, *17*, 764. (c) Li, W. Y.; Xu, L. N.; Chen, J. *Adv. Funct. Mater.* **2005**, *15*, 851.

(41) Xu, Z. P.; Zeng, H. C. *Chem. Mater.* **2000**, *12*, 3459.

(42) Cavani, F.; Trifiro, F.; Vaccari, A. *Catal. Today* **1991**, *11*, 173.

(43) Labajos, F. M.; Rives, V. *Inorg. Chem.* **1996**, *35*, 5313.

(44) Li, B. X.; Xie, Y.; Wu, C. Z.; Li, Z. Q.; Zhang, J. *Mater. Chem. Phys.* **2006**, *99*, 479.

(45) Hou, B.; Li, Z. J.; Xu, Y.; Wu, D.; Sun, Y. H. *J. Electroceram.* **2006**, *16*, 127.

(46) Yu, S. H.; Antonietti, M.; Cölfen, H.; Hartmann, J. *Nano Lett.* **2003**, *3*, 379.

(47) Chen, H. I.; Chang, H. Y. *Colloids Surf., A* **2004**, *242*, 61.

(48) Shen, H. K. *Organic Acid and Base*; Advanced Education Publishing Co., 1984, p 56. (b) He, Y.; Zhu, Y. F.; Wu, N. Z. *J. Solid State Chem.* **2004**, *177*, 2985.

(49) (a) Kniep, R.; Busch, S. *Angew. Chem., Int. Ed.* **1996**, *35*, 2624. (b) Busch, S.; Dolhaine, H.; DuChesne, A.; Heinz, S.; Hochrein, O.; Laeri, F.; Podebrad, O.; Vietze, U.; Weiland, T.; Kniep, R. *Eur. J. Inorg. Chem.* **1999**, *10*, 1643.

(50) (a) Pejova, B.; Isahi, A.; Najdoski, M.; Grozdanov, I. *Mater. Res. Bull.* **2001**, *36*, 161. (b) Meng, Y. D.; Chen, D. R.; Jiao, X. L. *J. Phys. Chem. B* **2006**, *110*, 15212.

(51) Jime'ne, V. M.; Ferna'ndez, A.; Espino's, J. P.; Gona'zlez-Elipe, A. R. *J. Electron Spectrosc. Relat. Phenom.* **1995**, *71*, 61.

(52) Huang, X. J.; Liu, J. H.; Shao, D. L.; Pi, Z. X.; Yu, Z. L. *Sens. Actuators, B* **2003**, *96*, 630.

CG8003068